


## Phase Structure of Electroweak Vacuum in a Strong Magnetic Field: The Lattice Results

M. N. Chernodub<sup>1</sup>, V. A. Goy<sup>2</sup>, and A. V. Molochkov<sup>2</sup>

<sup>1</sup>*Institut Denis Poisson UMR 7013, Université de Tours, 37200 Tours, France*

<sup>2</sup>*Pacific Quantum Center, Far Eastern Federal University, 690950 Vladivostok, Russia*

 (Received 1 August 2022; revised 19 December 2022; accepted 25 January 2023; published 16 March 2023)

Using first-principle lattice simulations, we demonstrate that in the background of a strong magnetic field (around  $10^{20}$  T), the electroweak sector of the vacuum experiences two consecutive crossover transitions associated with dramatic changes in the zero-temperature dynamics of the vector  $W$  bosons and the scalar Higgs particles, respectively. Above the first crossover, we observe the appearance of large, inhomogeneous structures consistent with a classical picture of the formation of  $W$  and  $Z$  condensates pierced by vortices. The presence of the  $W$  and  $Z$  condensates supports the emergence of the exotic superconducting and superfluid properties induced by a strong magnetic field in the vacuum. We find evidence that the vortices form a disordered solid or a liquid rather than a crystal. The second transition restores the electroweak symmetry. Such conditions can be realized in the near-horizon region of the magnetized black holes.

DOI: [10.1103/PhysRevLett.130.111802](https://doi.org/10.1103/PhysRevLett.130.111802)

Powerful magnetic-field background can modify the physical properties of the vacuum. For electromagnetic interactions described by quantum electrodynamics, the relevant intensity of the magnetic field is set by the Schwinger limit,  $B^{\text{QED}} = m_e^2/e \simeq 4 \times 10^9$  T [1] determined by the electron mass  $m_e$  [2]. At this strength—which is already bypassed by the fields near the surface of magnetars [3]—the vacuum acquires optical birefringence properties [4] and can act as a “magnetic lens” which can distort and magnify images [5] similarly to the celebrated galaxy-scale gravitational lengths.

Strong fundamental interactions, described by quantum chromodynamics, are affected by the magnetic field of the strength of the hadronic mass scale,  $B^{\text{QCD}} \sim m_p^2/e \sim 10^{16}$  T where  $m_p$  is the proton mass. Such fields generate the magnetic catalysis [6–8], which implies, in particular, a persistent enhancement of the chiral symmetry breaking in the QCD vacuum as the external magnetic field strengthens. The QCD vacuum can also acquire electromagnetic superconducting properties supported by condensation of electrically charged mesonic bound states with vector,  $\rho$ -meson quantum numbers [9]. The transient magnetic fields of relevant scales appear in noncentral and ultraperipheral heavy-ion collisions at RHIC and LHC facilities [10,11].

Electroweak fundamental interactions provide us with an additional source of vacuum instability at the critical magnetic field [12–14]:

$$B_{c1} \equiv B_{c1}^{\text{EW}} = \frac{m_W^2}{e} \simeq 1.1 \times 10^{20} \text{ T}, \quad (1)$$

determined by the mass  $m_W \simeq 80.4$  GeV of the  $W$  boson. It was suggested that this instability marks the onset of the condensation of the  $W$  bosons which can be inferred from the classical equations of motion of the electroweak model [13–18]. The condensate solution corresponds to a crystalline order of parallel vortexlike structures that shares geometric similarity with the lattice of Abrikosov vortices of a conventional type-II superconductor: for realistically heavy Higgs masses,  $m_H > m_Z$ , the vortices in the  $W$  condensate arrange themselves into a hexagonal lattice [15,19,20]. This exotic vacuum state should possess unusual anisotropic superconducting [9] and superfluid [21] properties [22]. The  $W$  condensation may also develop in the cores of electroweak strings [24–27].

The electroweak vacuum is suggested to experience the second transition at an even higher magnetic field:

$$B_{c2} \equiv B_{c2}^{\text{EW}} = \frac{m_H^2}{e} \simeq 2.7 \times 10^{20} \text{ T}, \quad (2)$$

determined by the Higgs mass  $m_H = 125.1$  GeV. Above  $B_{c2}$ , the electroweak symmetry should be restored [18,28,29]. In this phase, the vortex lattice evaporates leaving some traces in this new phase [30,31]. The magnetic fields of the relevant  $10^{20}$  T scale might have been created at the cosmological electroweak phase

---

Published by the American Physical Society under the terms of the [Creative Commons Attribution 4.0 International license](https://creativecommons.org/licenses/by/4.0/). Further distribution of this work must maintain attribution to the author(s) and the published article's title, journal citation, and DOI. Funded by SCOAP<sup>3</sup>.

transition in the first moments of the early Universe [32,33]. Such enormous fields were suggested to exist even in the modern Universe in the vicinity of the magnetized black holes [34,35].

Our Letter aims to establish, using the first-principle lattice simulations, the phase structure of the vacuum subjected to magnetic fields of the electroweak strength. Despite the “weak” name, such fields are among the most powerful magnetic fields that were rarely discussed in the context of the standard model of particles.

The discussions of the effect of magnetic fields on the vacuum structure reveal certain controversies in the literature. The transition to the inhomogeneous superconducting phase of the electroweak (EW) vacuum proceeds via the instability of the vacuum at the first critical field (1) because at  $B > B_{c1}$ , the ground state  $W$  mass becomes a purely imaginary quantity,  $m_W^2(B) = m_W^2 - |eB|$ . At the classical level, the formation of the periodic vortex lattice in the background magnetic field has been established in the EW model [36]. However, this classical-level scenario, together with the arguments based on loop computations [12], has been questioned in Ref. [37] where it was shown that quantum corrections could add a radiative term to the classical  $W$  mass in such a way that the mass does not vanish at the critical field  $B = B_{c1}$ . Consequently, it was concluded that no thermodynamic instability should occur in the electroweak sector. Earlier numerical simulations of the electroweak model in the background magnetic field did not reveal the presence of the vortex-dominated phase around the finite-temperature electroweak crossover [38] which could be explained by a destructive role of thermal fluctuations.

A similar no-go theorem was suggested to forbid the superconducting transition in QCD vacuum [39]. The instability in QCD should proceed via the spontaneous  $\rho$ -meson condensation similarly to the magnetic-field induced condensation of the  $W$  bosons in the EW model [9]. The fact that the  $\rho$ -meson mass does not vanish at any magnetic field was later supported by the effective model calculations [40] as well as the first-principle numerical simulations [41]. However, despite the absence of the thermodynamic singularity at finite magnetic field  $B$ , it was argued that the large- $B$  superconducting phase can still emerge via a smooth crossover transition implying that the transition to the new phase occurs at nonvanishing  $\rho$ -meson mass in the absence of a thermodynamic singularity [42]. The latter scenario has a speculative nature that requires confirmation from a first-principle simulation. To this end, the electroweak model provides us with an exciting playground, given the similarity of the superconducting mechanisms in both systems.

We consider the bosonic sector of the electroweak model with the Lagrangian

$$\begin{aligned} \mathcal{L}_{\text{EW}} = & -\frac{1}{2} \text{Tr}(W_{\mu\nu} W^{\mu\nu}) - \frac{1}{4} Y_{\mu\nu} Y^{\mu\nu} \\ & + (D_\mu \phi)^\dagger (D^\mu \phi) - V(\phi), \end{aligned} \quad (3)$$

where the field strengths of, respectively, the SU(2) gauge field  $W_\mu^a$  and U(1)<sub>Y</sub> hypercharge gauge field  $Y_\mu$  are

$$W_{\mu\nu}^a = \partial_\mu W_\nu^a - \partial_\nu W_\mu^a + ig\epsilon^{abc} W_\mu^b W_\nu^c, \quad (4)$$

$$Y_{\mu\nu} = \partial_\mu Y_\nu - \partial_\nu Y_\mu. \quad (5)$$

These vector fields interact with the complex scalar Higgs doublet  $\phi \equiv (\phi_1, \phi_2)^T$  via the covariant derivative:

$$D_\mu = \partial_\mu + \frac{i}{2} g W_\mu^a \sigma^a + \frac{i}{2} g' Y_\mu, \quad (6)$$

where  $\sigma^a$  ( $a = 1, 2, 3$ ) are the Pauli matrices. The ratio of the U(1) and SU(2) gauge couplings,  $g'/g = \tan \theta_W$ , defines the electroweak mixing (Weinberg) angle  $\theta_W$  fixed in experiments [43]:  $\sin^2 \theta_W \equiv 1 - m_W^2/m_Z^2 = 0.22290(30)$ .

The last term in the Lagrangian (3) is the potential  $V(\phi) = \lambda(\phi^\dagger \phi - v^2/2)^2$  of the Higgs field doublet  $\phi$ , where  $\lambda$  is the dimensionless self-coupling of the Higgs field and the only dimensionful parameter  $v$  sets the vacuum expectation value of the Higgs field.

In the broken phase, the Higgs field acquires the mass  $m_H = \sqrt{2\lambda}v$ . The theory possesses the massless photon,

$$A_\mu = W_\mu^3 \sin \theta_W + Y_\mu \cos \theta_W, \quad (7)$$

and three massive gauge bosons which include the electrically (off-diagonal) charged  $W$  bosons  $W_\mu^\pm = W_\mu^1 \pm iW_\mu^2$ , and the neutral (diagonal)  $Z$  boson:

$$Z_\mu = W_\mu^3 \cos \theta_W - Y_\mu \sin \theta_W, \quad (8)$$

with the masses  $m_W = gv/2$  and  $m_Z = m_W/\cos \theta_W$ .

We consider the electroweak vacuum in the background of the hypermagnetic field  $\mathbf{B}_Y = \nabla \times \mathbf{Y}$  corresponding to the hypergauge field  $Y^\mu = (Y^0, \mathbf{Y})$ . In the broken phase, the two fields are related to each other:

$$g' \mathbf{B}_Y = e \mathbf{B} \quad [\text{broken phase}], \quad (9)$$

as it follows from the definition of the elementary electric charge,  $e = g \sin \theta_W = g' \cos \theta_W = gg'/\sqrt{g^2 + g'^2}$ , Eqs. (7) and (8), as well as from the fact that in the broken phase, the  $Z$  boson is a massive particle which carries no global flux. In the symmetry-restored phase, where the magnetic field  $\mathbf{B}$  cannot be defined, the hypermagnetic field  $\mathbf{B}_Y$  plays a role of a genuine field.

Using the first-principle Monte Carlo techniques, we simulate the lattice version of the EW model (3). The standard lattice discretization of the model, the known particularities of the lattice (hyper)magnetic field, the technicalities related to the choice of lattice parameters close to continuum limit, and the lattice form of the physical observables discussed in the Letter are described

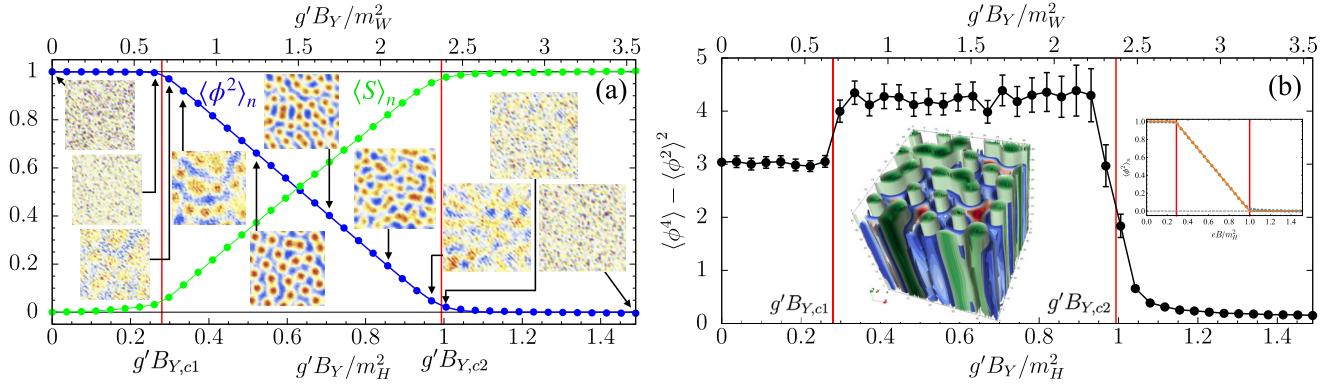


FIG. 1. (a) Normalized value  $\langle \phi^2 \rangle_n = \phi_r^2(B_Y)/\phi_r^2(0)$  of the additively renormalized, volume-averaged,  $\phi^2 \equiv (1/V) \int \phi^\dagger \phi$ , squared Higgs condensate  $\phi_r^2(B_Y) = \langle \phi^2(B_Y) \rangle - \langle \phi^2(\infty) \rangle$  (blue) and the likewise normalized action  $\langle S \rangle_n$  (green). The insets show the density plots of the  $Z_{12}$  fluxes in the cross sections normal to the magnetic field axis in typical configurations (more details are provided in the description of Fig. 3). (b) The susceptibility of the Higgs field squared vs the hypermagnetic field  $B_Y$ . The right inset shows the fit of the Higgs condensate shown in (a) by the piecewise function (12). The left inset illustrates a typical 3D configuration in the inhomogeneous phase in the (hyper)magnetic field background  $g' B_Y = eB = 1.1 m_W^2$  (the total number of vortices is 24). The equipotential surfaces of the  $W$  condensate (the Higgs condensate) are shown in blue and red (green). These quantities, which take their maximal values at the centers of the corresponding structures, are shown in complimentary regions. We used a cooling procedure to improve visibility of this 3D picture. The vertical red lines denote the transitions.

in Supplemental Material [44], Secs. A, B, C, and D, respectively. Important subtleties of definitions of fields and particle contents in the standard electroweak model and their lattice realizations are reviewed in Ref. [66].

In Fig. 1(a) we show the (normalized) vacuum expectation values of the Higgs field squared  $\langle |\phi|^2 \rangle$  and the action of the model—the EW Lagrangian (3) integrated over the whole spacetime—as the functions of the background (hyper)magnetic field  $g' B_Y$ . These observables point out to the existence of three phases separated by two pseudo-critical magnetic fields:

$$g' B_{Y,c1} \equiv e B_{c1} = 0.68(5) m_W^2, \quad (10)$$

$$g' B_{Y,c2} \equiv e B_{c2} = 0.99(2) m_H^2, \quad (11)$$

identified as the (pairwise coinciding) inflection points of the Higgs condensate and the action, supporting the gauge-invariant nature of the transitions.

The first critical field (10) turns out to be about 30% weaker than value (1) predicted by the classical theoretical analysis that does not take into account quantum fluctuations. However, the second critical field (11) agrees precisely with the theoretical value (2).

The classical picture predicts that the magnetic field affects the Higgs condensate as follows [12–19,28,29]: (i) In the broken phase ( $B < B_{c1}$ ), the Higgs condensate does not depend on the magnetic field  $B$ . (ii) When  $B$  exceeds the first critical value  $B = B_{c1}$ , the vacuum develops a raising  $W$  condensate which gradually inhibits the Higgs condensate. (iii) Finally, as the field reaches the second critical value,  $B = B_{c2}$ , the Higgs condensate

should vanish, and the electroweak theory should be restored.

All these properties are spectacularly confirmed in Fig. 1(a), where the fluctuations of scalar excitations of the condensate are removed by the normalization [76].

The observed dependence of the Higgs expectation value on magnetic field, shown in Fig. 1(a), can be described by an impressively simple piecewise-linear formula predicted by the theory [18,21,77,78]:

$$\frac{\langle \phi^2 \rangle_r(B)}{\langle \phi^2 \rangle_r(0)} = \begin{cases} 1, & B < B_{c1}, \\ \frac{B_{c2}-B}{B_{c2}-B_{c1}}, & B_{c1} < B < B_{c2}, \\ 0, & B > B_{c2}, \end{cases} \quad (12)$$

which fits our data everywhere except for small regions around the (pseudo)critical points  $B = B_{c1}$  and  $B = B_{c2}$ .

The structure of the classical solution around  $B_{c1}$  implies that the first phase transition should be of the second order [17,21]. In this case, the susceptibility of the Higgs field should possess a local maximum at the (pseudo)critical point. We do not see any peaks in the susceptibility across neither  $B_{c1}$  nor  $B_{c2}$ , Fig. 1(b). Thus, these transitions are smooth crossovers.

The  $W$  condensates are shown in Fig. 2. In an excellent qualitative agreement with the theory (the right inset), the squared  $W_\perp^2$  condensate raises linearly in the intermediate phase. The observed slope of the linear part,  $\partial |W_\perp|^2 / \partial(eB) \simeq 2.9$ , is about 30% larger than the slope predicted by the classical solution,  $\partial |W_\perp|^2 / \partial(eB) \simeq 2.1$  [21]. This deviation indicates the important role of the quantum fluctuations responsible also for the 30% shift of the first critical field  $B_{c1}$ . In the restored phase at  $B > B_{c2}$ ,

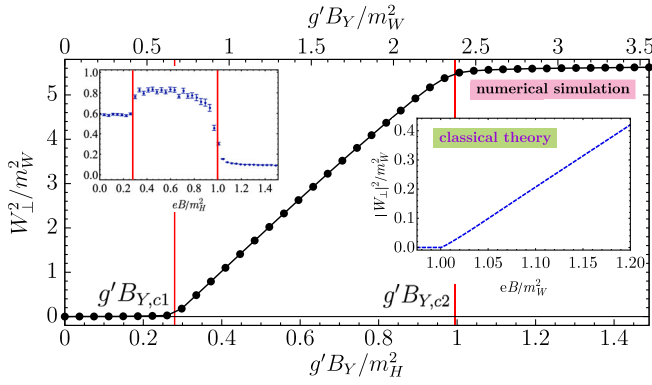


FIG. 2. Expectation value of the  $W$  condensate vs the (hyper) magnetic field  $g'B_Y = eB$ . The right inset is the theoretical result based on the classical solution for the transverse  $W$  condensate squared [21] around the first transition. The left inset shows the susceptibility of the transverse  $W$  condensate.

the  $W$  condensate flattens, possibly indicating the presence of the condensate of “zero-field twists” which are suggested to be the remnants of the vortex lattice [30] visible close to  $B = B_{c2}$  [31]. The  $W$  susceptibility (the left inset) exhibits close similarity with the susceptibility of the Higgs field shown in Fig. 1(b).

To confront our theoretical expectation with the first principle simulations, we visualize in Fig. 3 the structure of the electroweak fields in the cross-section perpendicular to

the magnetic field axis (we take  $\mathbf{B}$  in the  $z$  direction). We show analytical results in the classical theory in Figs. 3(a)–3(d) and visualize the numerical data obtained in lattice simulations in Figs. 3(e)–3(m). The numerical results were obtained by taking an average over a few dozen successive field configurations generated in the background of the (hyper)magnetic field  $g'B_Y \equiv eB \simeq 1.1m_W^2$  which corresponds to the intermediate phase in between two critical fields  $B_{c1} < B < B_{c2}$ .

According to the theoretical expectations [15,18,19], the ground state of the intermediate phase corresponds to a spatially inhomogeneous structure made of the  $W$  condensate with nonvanishing transverse components  $W_x$  and  $W_y$ . The inhomogeneities are produced by vortices that are embedded in the condensate. The vortices should arrange themselves into a hexagonal pattern in the plane perpendicular to the magnetic field. The transverse component of the  $W$  condensate,  $W_\perp = \sqrt{|W_x|^2 + |W_y|^2}$ , should vanish in the core of each vortex, Fig. 3(a).

Instead of the hexagonal pattern of the classical solution, Fig. 3(a), our lattice simulations reveal a less regular structure, Fig. 3(g). However, similarly to the classical solution, the lattice field  $W_\perp$  exhibits a semiclassical behavior characterized by coherent geometrical structures [79]. We associate these structures with the inhomogeneous  $W$  condensate. The condensate exhibits a set of separate deep minima which point to the presence of the vortex

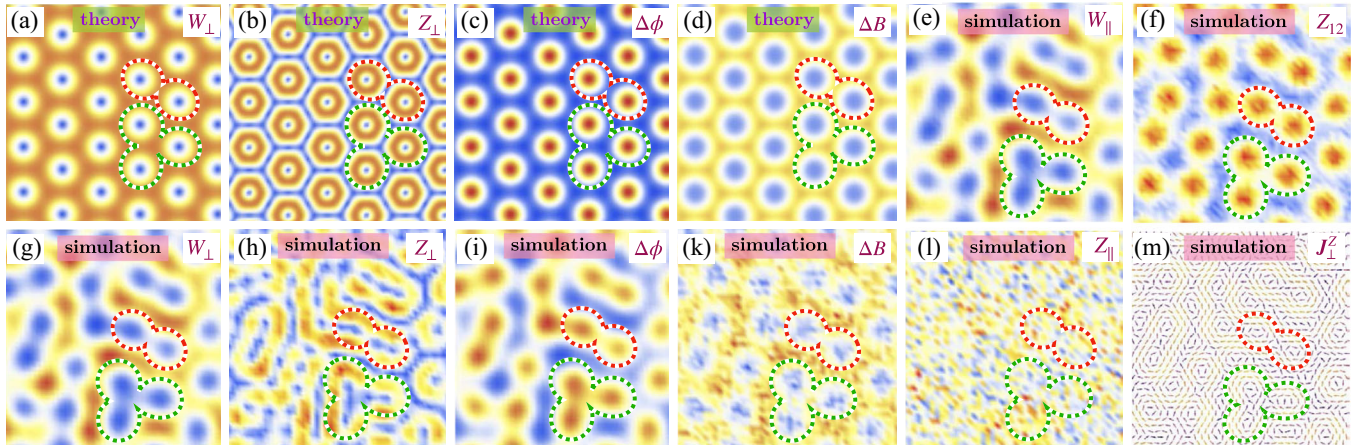


FIG. 3. Density plots of various quantities in the cross-sections normal to the axis of the (hyper)magnetic field. Theoretical results (a)–(d) are given for the classical solution of Ref. [21] at  $B = 1.01B_{c1}$ . The numerical results of the first-principle simulations, (e)–(m), are given for a typical lattice configuration in the background of the (hyper)magnetic field  $g'B_Y \equiv eB \simeq 1.1m_W^2 \simeq 1.6eB_{c1}$  (the magnetic number  $k = 12$  for our lattices). (a) and (g): transverse  $W$  condensate  $W_\perp = \sqrt{|W_x|^2 + |W_y|^2}$ ; (b) and (h): transverse  $Z$  condensate  $Z_\perp = \sqrt{|Z_x|^2 + |Z_y|^2}$ ; (c) and (i) local excess of the Higgs expectation value over the condensate,  $\Delta\phi(\mathbf{x}) = \phi(\mathbf{x}) - \langle\phi\rangle$ ; (d) and (k): local excess of the magnetic field value over the background,  $\Delta B(\mathbf{x}) = B(\mathbf{x}) - B_{\text{ext}}$ ; (e) and (l): longitudinal  $W$  and  $Z$  condensates,  $W_\parallel = |W_z|$  and  $Z_\parallel = |Z_z|$ , respectively (theoretically,  $W_\parallel = Z_\parallel = 0$  at the classical level); (f): the  $Z$  flux; (m) the neutral Higgs currents  $\mathbf{J}_\perp^Z$ . The red (blue) colors correspond to maxima (minima); absolute values are given for complex quantities. The same regions are circumvented by the red and green dashed lines (separately for the analytical solution and simulated configuration) to guide the eye. Each simulated picture is obtained by averaging data over a part of the Markov chain (last 5000 configurations). Averaging over the entire ensemble leads to blurring of the vortex structure.

cores in agreement with the theoretical classical picture, Fig. 3(a). Modulo occasional overlaps, the total number of vortices at chosen magnetic number  $k = 12$  appears to be equal to 24, which corresponds to the number  $2k$  of the elementary fluxes of hypermagnetic field, as expected.

Contrary to the expectations based on the classical theory, Fig. 3(a), the vortices do not form the crystalline phase in the vacuum, Fig. 3(g). While some traces of the crystalline vortex order are seen, the quantum fluctuations disorder the classical hexagonal structure so that the vortices form a disordered solid or, possibly, a liquid. The formation of the vortex liquid phase is not unexpected, though, as it has been proposed, in a similar non-Abelian context, in Ref. [80].

According to the classical picture, the transverse  $Z$  condensate  $Z_{\perp} = \sqrt{|Z_x|^2 + |Z_y|^2}$  forms a regular honeycomb structure, Fig. 3(b). This neutral condensate vanishes in the center of each vortex and a honeycomblike manifold in between the vortices. The regions with nonzero  $Z$  condensate are thin pipelike shells surrounding the vortex cores. Strikingly, these classical structures, disordered by quantum fluctuations, are also seen in our lattice configurations, Fig. 3(h): the thin shells of the  $Z$  condensate surround the cores of vortices.

The classical EW theory predicts that in the cores of vortices, the Higgs condensate should get enhanced [21], Fig. 3(c), while the magnetic field should be locally suppressed due to the antiscreening effect [14], Fig. 3(d). These properties, which defy our intuition based on the Abrikosov picture of type-II superconductors, are confirmed by the results of our numerical simulations shown in Figs. 3(i) and 3(k), respectively. A 3D picture of the Higgs and  $W$  condensates and the magnetic field lines of a typical configuration is shown in the inset of Fig. 1(b).

We also noticed that  $|W_x| \simeq |W_y|$  holds high precision in numerical simulations. The unexpected outcome of our simulations is the presence of the large longitudinal condensate  $W_{\parallel} \simeq W_{\perp}$ , Fig. 3(e) which closely mimics the transverse condensate, Fig. 3(g). This observation disagrees with the classical theory that predicts  $W_{\parallel} = 0$  in the ground state. On the contrary, the condensate of the  $z$  component of the neutral  $Z$  boson is vanishing in agreement with the classical picture: we observe only small quantum fluctuations in this quantity, Fig. 3(l).

Numerically, the  $Z_{12}$  flux provides us with the most transparent view of the vortex content of field configurations, Fig. 3(f). The peaks in the  $Z$  flux point out to the positions of the vortex cores also seen as the deeps in the  $W$  condensate, Fig. 3(e), the spikes in the Higgs condensate, Fig. 3(g), and, much less clear, as the minima in the magnetic field, Fig. 3(h). The associated neutral currents  $\mathbf{J}^Z$  of the Higgs field, Fig. 3(m), defined as a variation of the matter part of the action with respect to the  $Z$  field, circumvents the vortices.

In the inset of Fig. 1(a), we show the evolution of the  $Z$  flux density in the transverse plane of the gradually

increasing (hyper)magnetic field. The vortices start to form as soon as the magnetic field crosses the first pseudocritical value,  $B = B_{c1}$ . The vortex structures are barely seen. The fuzziness of vortex positions appears due to the weakness of the condensates right above the critical point. This property makes the weak classical structure vulnerable to the disorder caused by ultraviolet fluctuations and phonons in the vortex lattice that lead to the drifting of the vortex cores. The vortices may form a liquid close to the first critical field  $B_{c1}$ .

In the middle of the superconducting phase, the vortex liquid partially solidifies into a disordered solid. The physical motion of the vortices leads to enhanced local fluctuations of all physical quantities that experience extrema at or around vortex cores. In particular, the vortex motion enhances fluctuations of the Higgs condensate, thus leading to the elevated values of the Higgs and  $W$  susceptibilities in the inhomogeneous phase that we already observed in Figs. 1(b) and 2, respectively.

Close to the second critical field,  $B = B_{c2}$ , the vortex solid starts to melt. Finally, the vortices disappear entirely as the vacuum crosses into the third phase at  $B > B_{c2}$ , where the electroweak symmetry gets restored.

*Conclusions.*—Using first-principle numerical simulations, we establish the three-phase structure of the electroweak sector of the vacuum in the background of the strong magnetic field at zero temperature. In agreement with the theoretical analysis [12–19,28,29], we find that the vacuum experiences two successive transitions. Contrary to the expectations, these transitions are smooth crossovers.

As the magnetic field reaches the first pseudocritical value (10), the vacuum turns into the intermediate inhomogeneous phase, characterized by the presence of classically large  $W$  and  $Z$  condensates. Then, at the second pseudocritical field (11), the inhomogeneities disappear, and the electroweak symmetry gets restored. The formation of the disordered vortex solid and its evaporation with increasing magnetic field is shown in the Supplementary Video. The inhomogeneous phase is populated by vortices that locally have an almost classical field structure, mostly in agreement with Refs. [17,21]. The classical hexagonal order of the vortex phase is, however, not realized due to strong quantum fluctuations: we find the evidence that in the middle of the inhomogeneous phase, the vortices appear to form a disordered vortex solid which melts, closer to both pseudocritical magnetic fields, into a vortex liquid.

Summarizing, we have shown in first-principle calculations that the electroweak sector of the vacuum experiences two consecutive crossover transitions in strengthening magnetic field background. At intermediate fields in between these crossovers, we observe the appearance of large, inhomogeneous structures consistent with theoretically expected [13–18] a classical picture of the formation of  $W$  and  $Z$  condensates pierced by vortices that forms a disordered solid or a liquid rather than expected

solid. The presence of classically significant  $W$  and  $Z$  condensates points to the fascinating possibility that in the strong magnetic field, the vacuum becomes an electromagnetic superconductor enriched by a neutral superfluid component that supports dissipationless transport along magnetic field lines [9,21]. In the present time, such conditions can be realized in the vicinity of the magnetized black holes [34,35].

M. C. is grateful to M. Shaposhnikov for illuminating discussions. The numerical simulations were performed at the Supercomputer SQUID (Osaka University, Japan) and the computing cluster Vostok-1 of Far Eastern Federal University. V. G. has been supported by RSF (Project No. 21-72-00121 [81]). A. M. has been partially supported within the state assignment of the Ministry of Science and Higher Education of Russia (Project No. 0657-2020-0015). M. C. has been partially supported by the project IEA-International Emerging Actions No. 00677.

- 
- [1] We use the units  $\hbar = c = 1$ .
- [2] J. S. Schwinger, *Phys. Rev.* **82**, 664 (1951).
- [3] S. Olausen and V. Kaspi, *Astrophys. J. Suppl. Ser.* **212**, 6 (2014).
- [4] S. L. Adler, *Ann. Phys. (N.Y.)* **67**, 599 (1971).
- [5] N. J. Shaviv, J. S. Heyl, and Y. Lithwick, *Mon. Not. R. Astron. Soc.* **306**, 333 (1999).
- [6] S. P. Klevansky and R. H. Lemmer, *Phys. Rev. D* **39**, 3478 (1989).
- [7] K. G. Klimenko, *Z. Phys. C* **54**, 323 (1992).
- [8] I. A. Shovkovy, *Lect. Notes Phys.* **871**, 13 (2013).
- [9] M. N. Chernodub, *Phys. Rev. D* **82**, 085011 (2010).
- [10] V. Skokov, A. Y. Illarionov, and V. Toneev, *Int. J. Mod. Phys. A* **24**, 5925 (2009).
- [11] W.-T. Deng and X.-G. Huang, *Phys. Rev. C* **85**, 044907 (2012).
- [12] N. K. Nielsen and P. Olesen, *Nucl. Phys.* **B144**, 376 (1978).
- [13] V. Skalozub, *Sov. J. Nucl. Phys.* **28** (1978).
- [14] J. Ambjorn and P. Olesen, *Phys. Lett. B* **214**, 565 (1988).
- [15] V. V. Skalozub, *Sov. J. Nucl. Phys.* **45**, 1058 (1987).
- [16] J. Ambjorn and P. Olesen, *Nucl. Phys.* **B315**, 606 (1989).
- [17] J. Ambjorn and P. Olesen, *Phys. Lett. B* **218**, 67 (1989); **220**, 659(E) (1989).
- [18] J. Ambjorn and P. Olesen, *Nucl. Phys.* **B330**, 193 (1990).
- [19] S. W. MacDowell and O. Tornkvist, *Phys. Rev. D* **45**, 3833 (1992).
- [20] O. Tornkvist, [arXiv:hep-ph/9204235](https://arxiv.org/abs/hep-ph/9204235).
- [21] M. N. Chernodub, J. Van Doorselaere, and H. Verschelde, *Phys. Rev. D* **88**, 065006 (2013).
- [22] The vacuum superconductivity at QCD [9] and Electroweak [9,21] scales is similar to reentrant superconductivity which is suggested to occur in clean superconducting materials in very high magnetic fields [23].
- [23] M. Rasolt and Z. Tešanović, *Rev. Mod. Phys.* **64**, 709 (1992).
- [24] A. Achúcarro, R. Gregory, J. A. Harvey, and K. Kuijken, *Phys. Rev. Lett.* **72**, 3646 (1994).
- [25] W. B. Perkins, *Phys. Rev. D* **47**, R5224 (1993).
- [26] P. Olesen, [arXiv:hep-ph/9310275](https://arxiv.org/abs/hep-ph/9310275).
- [27] J. Garaud and M. S. Volkov, *Nucl. Phys.* **B826**, 174 (2010).
- [28] A. Salam and J. A. Strathdee, *Nucl. Phys.* **B90**, 203 (1975).
- [29] A. D. Linde, *Phys. Lett.* **62B**, 435 (1976).
- [30] P. Olesen, *Phys. Lett. B* **268**, 389 (1991).
- [31] J. Van Doorselaere, *Phys. Rev. D* **88**, 025013 (2013).
- [32] T. Vachaspati, *Phys. Lett. B* **265**, 258 (1991).
- [33] D. Grasso and H. R. Rubinstein, *Phys. Rep.* **348**, 163 (2001).
- [34] J. Maldacena, *J. High Energy Phys.* **04** (2021) 079.
- [35] D. Ghosh, A. Thalappilil, and F. Ullah, *Phys. Rev. D* **103**, 023006 (2021).
- [36] D. L. J. Ho and A. Rajantie, *Phys. Rev. D* **102**, 053002 (2020).
- [37] V. V. Skalozub, *Phys. At. Nucl.* **77**, 901 (2014).
- [38] K. Kajantie, M. Laine, J. Peisa, K. Rummukainen, and M. E. Shaposhnikov, *Nucl. Phys.* **B544**, 357 (1999).
- [39] Y. Hidaka and A. Yamamoto, *Phys. Rev. D* **87**, 094502 (2013).
- [40] M. A. Andreichikov, B. O. Kerbikov, V. D. Orlovsky, and Y. A. Simonov, *Phys. Rev. D* **87**, 094029 (2013).
- [41] G. S. Bali, B. B. Brandt, G. Endrődi, and B. Gläsel, *Phys. Rev. D* **97**, 034505 (2018).
- [42] M. N. Chernodub, *Phys. Rev. D* **89**, 018501 (2014).
- [43] E. Tiesinga, P. J. Mohr, D. B. Newell, and B. N. Taylor, *J. Phys. Chem. Ref. Data* **50**, 033105 (2021).
- [44] See Supplemental Material at <http://link.aps.org/supplemental/10.1103/PhysRevLett.130.111802> for a detailed description of the numerical procedures used in the first-principle lattice simulations implemented in the paper, which includes Refs. [45–75].
- [45] B. Bunk, E.-M. Ilgenfritz, J. Kripfganz, and A. Schiller, *Phys. Lett. B* **284**, 371 (1992).
- [46] B. Bunk, E.-M. Ilgenfritz, J. Kripfganz, and A. Schiller, *Nucl. Phys.* **B403**, 453 (1993).
- [47] Z. Fodor, J. Hein, K. Jansen, A. Jaster, and I. Montvay, *Nucl. Phys.* **B439**, 147 (1995).
- [48] Z. Fodor, J. Hein, K. Jansen, A. Jaster, I. Montvay, and F. Csikor, *Phys. Lett. B* **334**, 405 (1994).
- [49] F. Csikor, Z. Fodor, J. Hein, A. Jaster, and I. Montvay, *Nucl. Phys.* **B474**, 421 (1996).
- [50] Y. Aoki, F. Csikor, Z. Fodor, and A. Ukawa, *Phys. Rev. D* **60**, 013001 (1999).
- [51] A. D. Sakharov, *Pis'ma Zh. Eksp. Teor. Fiz.* **5**, 32 (1967), [http://jetpletters.ru/ps/1643/article\\_25089.shtml](http://jetpletters.ru/ps/1643/article_25089.shtml).
- [52] V. A. Rubakov and M. E. Shaposhnikov, *Usp. Fiz. Nauk* **166**, 493 (1996).
- [53] K. Kajantie, K. Rummukainen, and M. E. Shaposhnikov, *Nucl. Phys.* **B407**, 356 (1993).
- [54] E.-M. Ilgenfritz, J. Kripfganz, H. Perlt, and A. Schiller, *Phys. Lett. B* **356**, 561 (1995).
- [55] M. Gurtler, E.-M. Ilgenfritz, J. Kripfganz, H. Perlt, and A. Schiller, *Nucl. Phys.* **B483**, 383 (1997).
- [56] K. Kajantie, M. Laine, K. Rummukainen, and M. E. Shaposhnikov, *Nucl. Phys.* **B493**, 413 (1997).
- [57] K. Kajantie, M. Laine, K. Rummukainen, and M. E. Shaposhnikov, *Phys. Rev. Lett.* **77**, 2887 (1996).
- [58] M. D'Onofrio and K. Rummukainen, *Phys. Rev. D* **93**, 025003 (2016).
- [59] W. Langguth, I. Montvay, and P. Weisz, *Nucl. Phys.* **B277**, 11 (1986).

- [60] G. S. Bali, F. Bruckmann, G. Endrodi, Z. Fodor, S. D. Katz, S. Krieg, A. Schafer, and K. K. Szabo, *J. High Energy Phys.* **02** (2012) 044.
- [61] C. Gattringer and C. B. Lang, *Quantum Chromodynamics on the Lattice* (Springer, Berlin, 2010), Vol. 788, 10.1007/978-3-642-01850-3.
- [62] J. Frohlich, G. Morchio, and F. Strocchi, *Phys. Lett.* **97B**, 249 (1980).
- [63] J. Frohlich, G. Morchio, and F. Strocchi, *Nucl. Phys.* **B190**, 553 (1981).
- [64] R. M. Woloshyn, *Phys. Rev. D* **95**, 054507 (2017).
- [65] R. Lewis and R. M. Woloshyn, *Phys. Rev. D* **98**, 034502 (2018).
- [66] A. Maas, *Prog. Part. Nucl. Phys.* **106**, 132 (2019).
- [67] S. Durr, *Comput. Phys. Commun.* **172**, 163 (2005).
- [68] R. Workman *et al.* (Particle Data Group), *Prog. Theor. Exp. Phys.* **2022**, 083C01 (2022).
- [69] F. Csikor, Z. Fodor, and J. Heitger, *Phys. Rev. Lett.* **82**, 21 (1999).
- [70] K. Osterwalder and E. Seiler, *Ann. Phys. (N.Y.)* **110**, 440 (1978).
- [71] E. H. Fradkin and S. H. Shenker, *Phys. Rev. D* **19**, 3682 (1979).
- [72] T. Banks and E. Rabinovici, *Nucl. Phys.* **B160**, 349 (1979).
- [73] E. Seiler, [arXiv:1506.00862](https://arxiv.org/abs/1506.00862).
- [74] B. W. Lee and J. Zinn-Justin, *Phys. Rev. D* **5**, 3121 (1972).
- [75] W. Caudy and J. Greensite, *Phys. Rev. D* **78**, 025018 (2008).
- [76] Strictly speaking, the vanishing of the Higgs condensate at  $B > B_{c2}$  is not evident from the normalized condensate squared of Fig. 1(a) without an additional analysis. Indeed, the quantity  $\langle \phi^2 \rangle$  is affected by significant ultraviolet contributions which are always present in broken and unbroken phases. However, the homogenization of the  $W$  condensate observed above  $B_{c2}$  suggests that the Higgs condensate should be absent at  $B > B_{c2}$ .
- [77] J. Ambjorn and P. Olesen, *Int. J. Mod. Phys. A* **05**, 4525 (1990).
- [78] J. Ambjorn and P. Olesen, in 4th Hellenic School on Elementary Particle Physics (1992), pp. 396–406, [arXiv: hep-ph/9304220](https://arxiv.org/abs/hep-ph/9304220).
- [79] We do not perform any smoothening or cooling procedures that could drive our Monte Carlo configurations of Figs. 3(e)–3(m) closer to the classical regime.
- [80] J. Ambjorn and P. Olesen, *Nucl. Phys.* **B170**, 60 (1980).
- [81] <https://rscf.ru/project/21-72-00121/>.